Molecular Dynamics Study of the Solvation of Calcium Carbonate in Water

3 AUTHORS, INCLUDING:

Davide Donadio
University of California, Davis
109 PUBLICATIONS **4,020** CITATIONS

Molecular Dynamics Study of the Solvation of Calcium Carbonate in Water

Fabien Bruneval,* Davide Donadio, and Michele Parrinello

Computational Science, Department of Chemistry and Applied Biosciences, ETH Zurich, c/o USI Campus, Via Giuseppe Buffi 13, CH-6900 Lugano, Switzerland

We performed molecular dynamics simulations of diluted solutions of calcium carbonate in water. To this end, we combined and tested previous polarizable models. The carbonate anion forms long-living hydrogen bonds with water and shows an amphiphilic character, in which the water molecules are expelled in a region close to its C_3 symmetry axis. The calcium cation forms a strongly bound ion pair with the carbonate. The first hydration shell around the $CaCO_3$ pair is found to be very similar to the location of the water molecules surrounding $CaCO_3$ in ikaite, the hydrated mineral.

I. Introduction

The nucleation of calcium carbonate in water is of great interest for both life sciences and industrial processes. On one hand, calcium carbonate occurs in the shells and crusts of a variety of undersea animals[1] that can selectively produce different crystalline and amorphous hydrate forms by a process called biomineralization. On the other hand, the growth of solid calcium carbonate in hot water is a major concern in industrial processes,[2] and is also a problem in everyday life. The nucleation of calcium carbonate is a complex phenomenon that involves several intermediate stages and phase transformations at the nano- and microscale. In contrast with common salts, the solubility of $CaCO_3$ in water decreases as the temperature increases. Understanding the early stages of the nucleation of calcium carbonate from solution would thus shed light on a process that is of as much fundamental interest to life sciences as it is to technology. Surprisingly, very little information is available, even about the properties of the building blocks of $CaCO_3$ in water. In particular, the hydration properties of CO_3^{2-} and, more generally, of complex doubly charged anions have not yet been elucidated. Small droplets of water of sulfate and oxalate have been studied,[3] but carbonate remains unexplored experimentally. This is the typical case, where computer simulations can provide useful information. Only recently have the first theoretical works become available for sulfate[4] and for carbonate at particularly high concentrations.[5] A study of the carbonate ion in water at low concentrations is still lacking. In contrast, much attention has been devoted to Ca^{2+} in water both theoretically[6−10] and experimentally.[11,12]

The present paper proposes to draw a clear picture of the solvation properties of the ions involved in calcium carbonate mineral nucleation. Since the system size required to describe the water shells around the ions is large, and since the simulation time needed to evaluate the dynamical properties is long, we have chosen to perform a classical molecular dynamics (MD) study, using empirical polarizable force fields.

Because of industrial interest in the behavior of calcium carbonate in hot water and in a strongly basic environment (pH > 10), we are going to focus on the 300−365 K temperature range and shall not consider the presence of HCO_3^- anions,

which, in turn, would be predominant in neutral and acid environments.

The paper is organized as follows: In the next section we describe the force field and prove its transferability to hydrated mineral forms of $CaCO_3$. The properties of the solvated calcium and carbonate ions are discussed in Section III, and, in Section IV, the formation and dissociation of a $CaCO_3$ pair are investigated as well as its solvation shell. The results are briefly summarized and discussed in Section V.

II. Building and Assessing the Force Field

Building an empirical force field for classical MD simulations of calcium carbonate in water is not a straightforward task. The main issue is the transferability of the potential to the different phases of calcium carbonate (calcite, aragonite) and to the hydrate forms. In addition, the model must provide a good description of the structural and dynamical properties of water, and of the interaction between Ca^{2+}, CO_3^{2-}, and H_2O. A force field parametrized for similar systems has been proposed by de Leeuw and Parker.[13,14] Since it was tuned to reproduce the interaction of water with mineral surfaces, this empirical potential gives a poor description of liquid water. Within this model, the oxygen−oxygen pair correlation function is much more structured than the experimental one at the same temperature (e.g., the height of the first peak is 3.8, compared to 2.8 from neutron diffraction[15]). As a consequence, the theoretically calculated self-diffusion coefficient is about half of the experimental value, which would qualitatively and quantitatively affect the dynamics and the solvation properties of the ions. Their force field was not intended to describe the ions in solution but rather the calcite/water interfaces. For the purpose of studying solvated species, we need a more realistic force field for water.

Our approach is hence to build, following the prescription from ref 13, a force field for the interaction between $CaCO_3$ and water, but using for water and calcium carbonate recently published potentials that better reproduce the properties of these systems.

A. The Force Field. Given the importance of calcite and aragonite in geology, several efficient force fields that describe the calcium carbonate minerals have been developed. Already in the early stages of this development, the explicit treatment of the polarization effects on the oxygen atoms has been

---

* Corresponding author.

TABLE 1: Parameters of the Empirical Force Field

interaction type	bond	coefficients										
		D (eV)	A (Å^{-1})	ρ (Å)	K (eV/rad^2)	θ_0	K (eV/Å^2)	x_0	A (eV)	C (eV Å^6)	ϵ (eV)	q (e)
					Intramolecular Potentials							
Morse	$C-O_c$	5	2.5155	1.20246								
harmonic angle	O_c-C-O_c				4.00	120°						
harmonic out-of-plane	$C-O_c-O_c-O_c$						12.68	0				
harmonic core–shell	O_c-O_c shell						52.740087					
	O_w-O_w shell						43.3275					
					Intermolecular Potentials							
Buckingham	O_c shell$-O_c$ shell			0.198913					64242.454	21.84357		
	$Ca-O_c$ shell			0.289118					2154.06	0		
	$Ca-C$			0.120000					1.2 10^8	0		
	$C-O_c$ shell			0.195838					2304.2385	0		
	$Ca-O_w$ shell			0.297000					1186.492877	0		
	O_c shell$-O_w$ shell			0.215172					12534.455133	12.09		
	O_c shell$-H$			0.230000					396.320957	0		
Lennard–Jones	O_w-O_w			3.18395							9.14665 10^{-3}	
electrostatics	Ca											2.000000
	C											1.343539
	O_c											1.018487
	O_c shell											−2.133000
	O_w											1.716360
	O_w shell											−1.716360
	H											0.55733
	D											−1.11466

recognized as essential.[16] Without a proper polarization term, the transferability of the fitted potential from aragonite to calcite would indeed be problematic.[16] The transferability issue is even more prominent in the present study, where the carbonate ions would experience very different local electrostatic fields, as they may be surrounded by either Ca^{2+} or H_2O or a combination of them. In the classical force field framework, the polarization of the electrons can be introduced in an empirical manner, through a massless negatively charged shell linked to its corresponding core via a harmonic spring.

Archer and co-workers[17] developed a polarizable model for calcium carbonate, which was parametrized on the experimental, structural, and elastic properties of both aragonite and calcite. In the present study, we use the functional forms and parameter values of ref 17 to mimic the interaction between Ca^{2+} and CO_3^{2-}. However, at times we felt the need to refine some of the parameters. This can be seen in Table 1, where most of the parameters are identical to those of ref 17, with the exception of the planar angle and the out-of-plane force constants for the carbonate anion, which required some more fine-tuning. In fact, in our earlier attempts to simulate the solvated anion, we realized that the CO_3^{2-} unit was not rigid enough to prevent the anion from bending and eventually collapsing. It is not surprising that a force field fitted to give the correct structure for minerals is not sensitive enough to the internal stiffness of a single ion.

We therefore carry out a fit of the angular force constant of the carbonate against ab initio data. The first principle calculations are performed on the isolated ion CO_3^{2-} at the MP2/6-311+G* level of theory using the Gaussian 03 code.[18] The CO_3^{2-} anion is not electronically stable in the gas phase, since the highest occupied molecular orbital (HOMO) lies above the vacuum level. Nevertheless, using the previously described localized basis set, the geometry can be readily obtained. The work of Stefanovitch et al.[19] validates this procedure: employing an implicit solvent model stabilizes the HOMO, but does not yield any change in the structural properties with respect to the gas-phase result. In Figure 1, we report the energetic cost of twisting in plane a $C-O_c$ bond with angle θ in panel a, and of

bending the ion with an out-of-plane distance x in panel b. As shown in the plots, the existing parametrization (dashed line) was not optimal with respect to the MP2 calculation (crosses), while the new parameters, reported in Table 1, display a much better agreement (solid lines in Figure 1). The in-plane harmonic force constant is doubled, and the out-of-plane one is increased by about 50%, which makes the anion much stiffer. Finally, we also introduce an additional short-ranged repulsion term $C-O_w$ with respect to ref 17, which prevents Ca and C from getting too close to one another at high pressures or high temperatures, but vanishes very fast with the Ca–C distance. Whenever necessary, we distinguish the oxygen from carbonate ions, labeled O_c, from the oxygen of water molecules, labeled O_w.

Consistently with the choice of using a shell model to mimic the polarizability of O_c, we choose to treat water at the same level. We therefore employ the polarizable model for water of Lamoureux et al.[20] This model, named SWM4-NDP, is an evolution of the TIP4P model.[21] The water molecules are treated as a rigid body with fixed O_w-H length (0.9572 Å) and $H\widehat{O_w}H$ angle (104.52°). A dummy point charge is added along the symmetry axis of the molecule in order to account for the permanent dipole moment of water. In addition to this TIP4P-like model, the SWM4-NDP force field has a charged shell attached to the O_w atom. The O_w shell and core have opposite charges and therefore account for the effect of a varying dipole. The short-range water–water interaction is dealt with by a Lennard–Jones potential centered on the O_w cores. The present model has been shown to give very accurate values for a wide range of properties of water.[20] In particular, the O_w-O_w pair correlation function closely reproduces the neutron diffraction data, and the self-diffusion coefficient is similar to the experimental value of 2.3×10^{-5} cm^2/s.

The last part of the force field has to deal with the interaction between Ca^{2+} CO_3^{2-} and H_2O. Following de Leeuw and Parker,[14] this interaction is modeled through a Buckingham functional form, and their parameters are used. As a stringent

Solvation of Calcium Carbonate in Water

J. Phys. Chem. B, Vol. 111, No. 42, 2007 **12221**
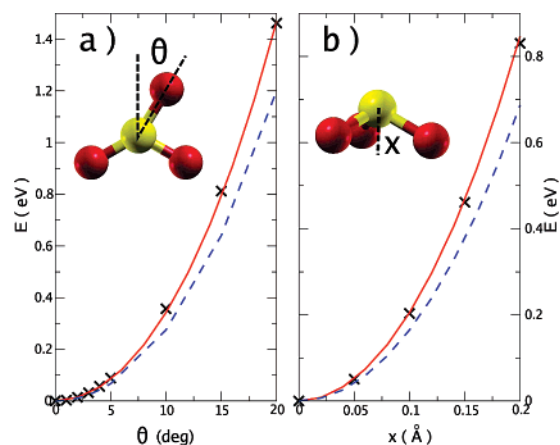
Figure 1. Energetic cost in eV of (a) twisting an in-plane angle θ of a $C-O_c$ bond of CO_3^{2-}; (b) bending the planar ion CO_3^{2-}, so that the carbon is distant by x from the plane formed by the oxygens. The crosses correspond to the MP2/6-311+G* calculations, the dashed lines correspond to the original empirical parameters, and the solid line corresponds to our refined parameters.

TABLE 2: Gas-Phase Binding Energy and Equilibrium Distance of Pairs within MP2/6-311+G* and within the Empirical Force field[a]

	MP2/6-311+G*		classical force field	
	U (eV)	d_{eq} (Å)	U (eV)	d_{eq} (Å)
$Ca^{2+} + H_2O$	−2.630	2.27	−2.058	2.31
$CO_3^{2-} + H_2O$	−1.514	3.16	−1.484	2.98
$Ca^{2+} + CO_3^{2-}$	−23.137	2.52	−22.169	2.66
$K^+ + CO_3^{2-}$	−9.833	2.81	−9.596	2.84
$K^+ + H_2O$	−0.937	2.59	−0.798	2.59

[a] The equilibrium distance d_{eq} stands for $Ca-O_w$ in the first row, for $C-O_w$ in the second row, for $Ca-C$ in the third row, for $K-C$ in the fourth row, and for $K-O_w$ in the last row.

test of our model, we consider the following pairs in vacuum: $Ca^{2+} + H_2O$, $CO_3^{2-} + H_2O$, and $Ca^{2+} + CO_3^{2-}$, and we compare them against first-principle calculations at the MP2/6-311+G* level. In the ab initio calculations, the geometry of the water molecules has been constrained to be that of the classical force field. All the other degrees of freedom have been relaxed at 0 K, both in ab initio and in classical approaches. In Table 2, we provide the binding energy and equilibrium distance of pairs using either the classical force field or our ab initio data. The differences lie within 0.15 Å for the equilibrium distances and within 0.5 eV for the binding energies. This is within the typical accuracy of shell models for the equilibrium distances, but it is larger than expected for the binding energies.[22] Attempts to further improve the force field were not successful because of the correlation between the different parameters of the Buckingham functional form.

B. Mineral Calculations. In order to check the transferability of the force field, we consider several minerals containing calcium carbonate and possibly water. In principle, the Ca^{2+} CO_3^{2-} force field is just slightly modified with respect to the original parametrization of Archer et al., thus we do not expect large discrepancies between our potential and that of ref 17 for the pure calcium carbonate minerals calcite and aragonite. In fact, the structural parameters of calcite and aragonite as obtained from our classical calculation at 0 K (Table 3) are very close to both the values of ref 17 and the experimental ones.

For our purposes, the calculation of hydrated $CaCO_3$ minerals is a more crucial test for our force field. We therefore consider the monohydrocalcite, $CaCO_3$ H_2O, and the hexahydrocalcite or ikaite, $CaCO_3$ $(H_2O)_6$. The equilibrium structure parameters

TABLE 3: Structural Parameters of Several Minerals Containing Calcium Carbonate, Hydrated or Not[a]

mineral name	parameter	classical force field	expt
calcite	volume (Å³)	226.22	226.91[23]
	a (Å)	5.71	5.74[23]
	b (Å)	4.96	4.96[23]
	c (Å)	7.99	7.97[23]
aragonite	volume (Å³)	368.84	368.07[23]
	a (Å)	4.98	4.99[23]
	b (Å)	4.98	4.99[23]
	c (Å)	17.08	17.06[23]
monohydrocalcite	volume (Å³)	712.34	727.73[24]
	a (Å)	10.39	10.55[24]
	b (Å)	10.39	10.55[24]
	c (Å)	7.62	7.54[24]
ikaite	volume (Å³)	733.37	754.07[25]
	a (Å)	8.56	8.79[25]
	b (Å)	8.32	8.31[25]
	c (Å)	11.00	11.02[25]
	β	108.09°	110.53°[25]

[a] The calculated parameters are compared to the experimental data from refs 23−25.

at 0 K are provided in Table 3. For both hydrated minerals, agreement with the X-ray diffraction data is very good. In particular, ikaite does not display any distortion of the unit cell in contrast to earlier force fields, which gave a shorter a axis and a longer c axis.[26]

This establishes the reliability of the empirical force field summarized in Table 1, which is capable of accurately describing pairs of molecules in the gas phase, pure liquid water, several crystalline phases of calcium carbonate, and hydrated calcium carbonate. Thus we can safely argue that the force field described so far is transferable and accurate enough to provide reliable simulations of the solvation of the Ca^{2+} and CO_3^{2-} ions in water.

C. Simulation Details. The classical MD runs are performed using a modified version of the DL_POLY code.[27,28] We carry out constant pressure−constant temperature (NPT) runs for equilibration and constant volume−constant temperature (NVT) runs for collection of data. For the NVT simulations, we employ the recently developed thermostat of Bussi et al.[29] This thermostat efficiently samples the canonical ensemble, and it is largely insensitive to the value of the coupling parameter between the system and the thermostat, which is expressed as a relaxation time. Even though this procedure is stochastic, it does not break the local dynamical correlations, since it acts only on the total kinetic energy. In the present work, for the runs aimed at calculating static properties, such as pair correlation functions and free energy, a short thermostat relaxation time (0.2 ps) was used. For runs collecting dynamical data, such as diffusion coefficients and correlation functions, a longer relaxation time (2 ps) was employed in order to minimize interference with the Newtonian dynamics of the system.

The dynamics of the shell model can be treated with two different approaches. As the shells are massless, they should, in principle, always relax instantaneously to the minimum of the potential energy. The "relaxed shell model" follows this spirit: the force acting on the shell is minimized at each time step to the zero-force point. This is somehow analogous to the Born−Oppenheimer version of ab initio MD. On the other hand, "adiabatic shell dynamics" is performed in the same spirit as Car−Parrinello MD,[30] where a finite mass is attributed to the in-principle massless shells. Their positions and velocities are obtained by integrating an equation of motion.[31] The advantage of this method is that the self-consistent relaxation of the shells is totally circumvented. We have also investigated an alternative

method, which proposes to evolve the massless shells using a time-reversible predictor−corrector algorithm.[32] This scheme has, in principle, the same efficiency as the Car−Parrinello-like approach.

We have carefully compared the performance of the last two approaches on a 270 water molecule system for 0.1 ns NVT runs, using the polarizable water model SWM4-NDP.[20] In the framework of Bussi et al.,[29] a conserved quantity, analogous to a total energy, can be defined even in NVT simulations. The constancy in this quantity is a measure of how accurately the canonical distribution is sampled. We have verified that both the predictor−corrector using as history the four previous positions and the Car−Parrinello-like schemes allow for an integration time step as large as 1 fs. Using this time step, the drift of the conserved quantity remains low for the predictor−corrector, but is as much as two times lower for the Car−Parrinello-like shell approach. As a consequence, we make use of the adiabatic shell model in all of the following.

Because of the nonzero mass in the adiabatic shell model, one should nevertheless consider the energy transfer from the "hot" atoms to the "cold" shells. This heat flux is controlled by the overlap of the respective eigenmodes of the two subsystems. When the mass of the shells is small enough (here we consider $m_s = 0.3$ a.u. for both O_w shells and O_c shells), this flux can be made small. In order to keep the temperature of the shell close to 0 K, we have implemented a very simple zero temperature thermostat consisting of a damping of the shell velocities using the same coupling time as that for the thermostat of the "hot" atoms. This thermostat is formally equivalent to a Langevin thermostat at 0 K. We checked that the temperature of the shells remains close to 0 K while the atoms are sampling the correct canonical ensemble.

The equations of motion were integrated using a velocity Verlet algorithm with a 1 fs time step, periodic boundary conditions were employed, and smooth particle mesh Ewald was used to evaluate the long-range Coulomb interactions. van der Waals interactions were cut off beyond the distance of 8 Å.

III. Solvated Ions

In this section we shall study the solvated ions using the force field presented previously. The properties of the solvation shell of Ca^{2+} have already been studied using both ab initio and classical MD.[6−10] Despite the fact that the simulation times are relatively short (40 ps), the available first principle results will validate the accuracy of the force field parametrization. At the same time, our classical MD simulations will provide valuable information about the dynamical properties of Ca^{2+} in water for longer simulation times.

The solvation of complex dianions is, in general, a much less visited topic. Few experimental data are available. In the case of the carbonate ion, practical considerations preclude straight-forward experiments: the carbonate concentration should be very low so as to avoid precipitation, and the HCO_3^+/CO_3^{2-} conjugated pair is a weak acid with $pK_a = 10.3$, which means that the experiments should be performed in very alkaline solutions in order to have a preponderance of carbonate over bicarbonate. From the theoretical point of view, very few calculations can be found for complex dianions.[4] In particular, to the best of our knowledge, a single classical MD study of CO_3^{2-} in water has been performed so far.[5]

The MD runs presented in this section were performed on periodic systems consisting of a single ion and 262 water molecules in a cubic box. The neutrality of the box is enforced by a uniform neutralizing background. The size of the box is
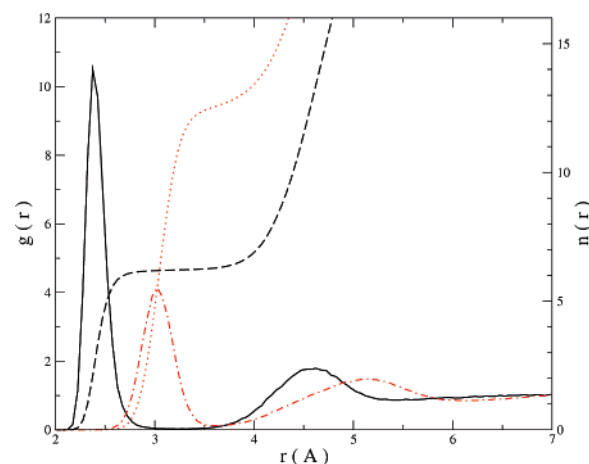
Figure 2. Pair correlation function $g(r)$ of Ca and O_w (solid line), and of Ca and H (dot-dashed line) at 300 K (scale on the left). The corresponding running integration numbers $n(r)$ are displayed by a dashed line for Ca−O and a dotted line for Ca−H (scale on the right).

equilibrated during an NPT run. Its side length is around 20 Å, depending on the temperature, which yields a molar concentration of 0.2 M.

The pair correlation functions of Ca^{2+} with O_w and H provided in Figure 2 are obtained from a 0.5 ns NVT simulation at 300 K. The first peak is located at 2.39 Å for $Ca−O_w$ and at 3.03 Å for Ca−H. This compares very well with the Car−Parrinello MD results of ref 9, which were respectively 2.43 Å and 3.03 Å. The same agreement holds for the coordination number of Ca^{2+}: our calculation and the Car−Parrinello simulation both give 6.2 first neighbors. These findings are fully supported by neutron diffraction experiments[11] and extended X-ray absorption fine structure (EXAFS) measurements.[12] The experimental average $Ca−O_w$ distance is 2.43 Å, the Ca−H distance is 2.97 Å, and the coordination number is 7.2 ± 1.2. This gives a further assessment of the quality of the force field used here for the water solution, since it lies within the error bar of the experimental data.

The possibility of a long simulation time can give access to the dynamical properties of the hydration shell of Ca^{2+}. We can estimate the residence time of a water molecule in the first shell of calcium ions. Let us define the characteristic function h_{CaO_w}, the value of which is 1 when the Ca−O_w distance is lower than 3.5 Å and 0 elsewhere. We evaluate the h autocorrelation function as

$$C(t) = \frac{1}{N_{O_w}} \sum_{O_w} \langle \tilde{h}_{CaO_w}(0) \tilde{h}_{CaO_w}(t) \rangle \qquad (1)$$

where the sum runs over the oxygen atoms of all water molecules, and the deviation function $\tilde{h}_{CaO_w} = h_{CaO_w} - \langle h_{CaO_w} \rangle / N_{O_w}$ is introduced in order to remove the spurious correlation due to the finite simulation box. We then extract the average residence time τ by evaluating

$$\tau = \frac{\int dt C(t) t}{\int dt C(t)} \qquad (2)$$

From 10 ns simulations at 300 and 365 K, we produce the correlation functions in Figure 3. First, in calculating the functions h_{CaO_w}, we obtain the average coordination number of Ca^{2+}: 6.2 at 300 K and 6.3 at 365 K, which is consistent with the value just extracted from the pair correlation function.

Solvation of Calcium Carbonate in Water

J. Phys. Chem. B, Vol. 111, No. 42, 2007 **12223**
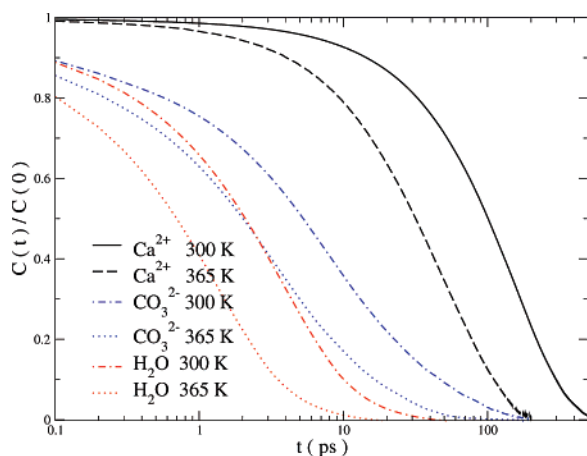
Figure 3. Normalized time correlation function of the residence in the first hydration shell of Ca^{2+} (black solid line for 300 K and black long dashed line for 365 K). Normalized time correlation function of the hydrogen bonds formed by $O_c\cdots H-O_w$ (blue dot-dashed line for 300 K and blue dotted line for 365 K). Normalized time correlation function of the hydrogen bonds formed in water by $O_w\cdots H-O_w$ (red dot-dashed line for 300 K and red dotted line for 365 K).

Figure 4. Pair correlation function $g(r)$ of O_c and O_w (solid line), and of O_c and H (dot-dashed line) at 300 K (scale on the left). The corresponding running integration numbers $n(r)$ are displayed with a dashed line for O_c-O_w and a dotted line for O_c-H (scale on the right).

Second, the two correlation functions of Figure 3 are quite simple. They show a single main time scale, as they are rather well fitted by a single-exponential function. Making use of eq 2, we evaluate that the water molecules remain coordinated to the calcium ion for 122 ± 10 ps at 300 K and 40 ± 4 ps at 365 K. The long residence time is explained by the strong Coulomb attraction produced by the doubly positively charged calcium ion. This typical time is consistent with quasielastic neutron scattering, which provides a value of around 100 ps.[33] Previous theoretical estimates of this quantity range from 700[34] to 10 ps.[6,8,9] The smallest value comes from first-principles MD and might suffer from the short simulation time affordable in this scheme.

The strong binding of Ca^{2+} with its local environment is expected to hinder its self-diffusion: when the calcium ion diffuses, it has to either break the strong bonds with the water of the first shell or drag its solvation shell along its trajectory. From 12 ns-long NVT runs, we evaluate the self-diffusion coefficient to be $0.58 10^{-5} cm^2 \cdot s^{-1}$ at 300 K and $1.79 10^{-5} cm^2 \cdot s^{-1}$ at 365 K. The value at room temperature is in close agreement with that of ref 34, $0.54 10^{-5} cm^2 \cdot s^{-1}$. The diffusion coefficient of Ca^{2+} is much lower than that of water, even taking into account the difference in the respective masses. This reflects the rigidity of the environment of the calcium ion.

In contrast to the calcium ion, the hydration shell of the carbonate anion has been much less studied. To provide a better understanding of its structure, we display the pair correlation function of O_c-O_w and O_c-H in Figure 4 for a temperature of 300 K. The first peak of the O_c-O_w and O_c-H pair correlation function are located respectively at 2.69 and 1.78 Å. The number of nearest-neighboring hydrogen atoms obtained from the integration of the first shell peak of the pair correlation function is 4.3.

To gain some more insight, it is instructive to build a three-dimensional map of the location of water molecules surrounding the carbonate ion following the representation used in ref 35. Figure 5 displays several isoprobability surfaces obtained from a 10 ns MD run. In Figure 6, the same information is recast in the form of a cut along a plane perpendicular to the carbonate ion passing through a C–O line. The location of water molecules in the first hydration shell lies preferably between or on top of and below the oxygens of the carbonate ion, in positions labeled
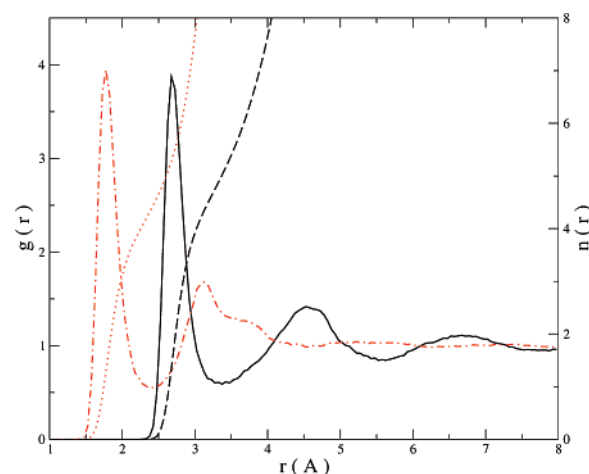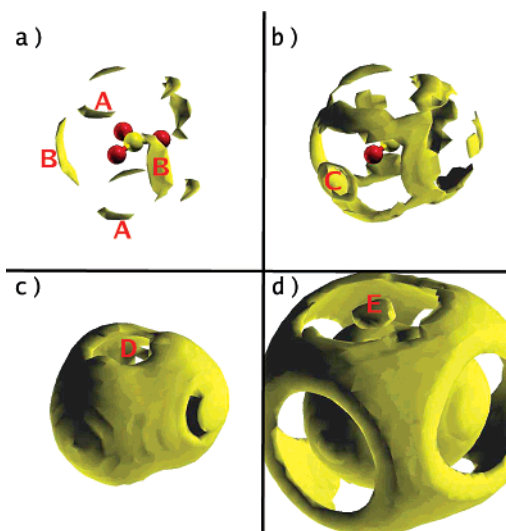

Figure 5. Isoprobability surfaces for the localization of O_w in the frame centered on the CO_3^{2-} anion. Positions A to E are defined in the text.

A and B in panel a of Figures 5 and in Figure 6. Then less probably, they lie straight in front of the O_c, in position C of panel b of Figure 5 and in Figure 6. A very interesting feature is that an exclusion area can be detected in the first hydration shell, located vertically from the carbon atom (position D in panel c of Figure 5 and in Figure 6). The water molecules are literally expelled from this region. The carbonate ion clearly displays hydrophilic and hydrophobic regions. This hydrophobic location may play a role in the nucleation of calcium carbonate in water: indeed the stacking of the CO_3^{2-} and Ca^{2+} may be an attempt to reduce as much as possible the contact between the hydrophobic region and the surrounding water. Indeed, if two carbonate anions associate on top of one another, such a configuration would minimize the contact between the hydrophobic part and water. This type of configuration is precisely the one adopted in two of the three common calcium carbonate minerals, aragonite and vaterite. As a consequence of the void created in the first hydration shell in position D, the second shell shows a high-density region in the vicinity of the hole of the first shell in the position labeled E in panel d of 5 and in Figure 6. One can note the neat separation between the first and second shells.
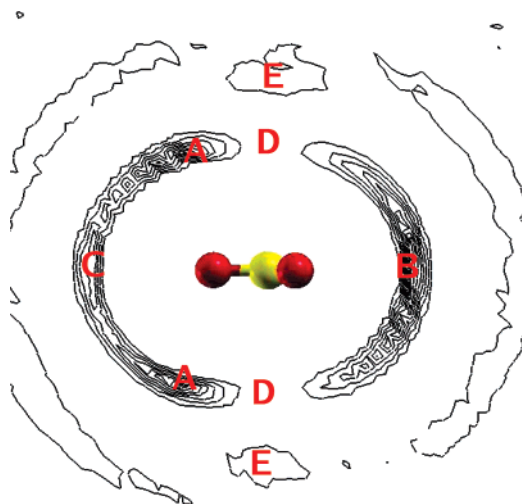
Figure 6. Probability isolines for the localization of O_w in a plane orthogonal to the carbonate and passing through a C–O line. Positions A to E are defined in the text.

Figure 7. Free energy profile in units of kT as a function of the distance between Ca and C, calculated for a Ca^{2+}/CO_3^{2-} pair with 100 water molecules at 300 K. The thick solid line is obtained from umbrella sampling, and the three other lines are from Jarzynski averages (see text).

Because of the negative charges located on the oxygen atoms of carbon, long-lived hydrogen bonds are formed between water and carbonate. These strong hydrogen bonds have a crucial influence on the dynamic properties of the solvated CO_3^{2-} ion. We consider a geometrical definition for the hydrogen bond: let the function $h_{O_wO_c}$ be equal to 1 if both conditions on the distance $|r_{O_w} - r_{O_c}| < 3.2$ Å and on the angle $\widehat{O_cO_wH} < 36°$ are satisfied, and 0 otherwise. Geometrical and energetic definitions have been shown to be almost equivalent for water.[36] The mean value $\langle h_{O_wO_c} \rangle$ gives the average number of hydrogen bonds formed per oxygen of carbonate: 4.03 at 300 K and 3.87 at 365 K. The correlation functions $C(t)$ at 300 and 365 K are reported in Figure 3. These functions show the typical aspect of hydrogen bond correlation functions,[36] which differs largely from the shape of the first shell correlation function of Ca^{2+}. As a comparison, we also draw in Figure 3 the correlation functions of the hydrogen bonds in water. These functions are obtained from a 1 ns run of 262 water molecules at 300 and 365 K. This allows us not only to elucidate the hydrogen bond properties, but also to provide the first evaluation of the relaxation time of hydrogen bonds for the very accurate SWM4-NDP model.[20] We use the definition of ref 37 and register a hydrogen bond whenever $|r_{O_w} - r_{O_w}| < 3.5$Å and $\widehat{O_wO_wH} < 30°$.

In the SWM4-NDP model, each water molecule forms, on average, 3.62 hydrogen bonds at 300 K and 3.28 at 365 K. The relaxation time of the hydrogen bonds, as evaluated through eq 2, is 6.1 ps at 300 K and 2.1 ps at 365 K. The value at 300 K is smaller than the value of 12 ps obtained with TIP5P.[38] This is in agreement with the statement that the TIP5P model with point charges located on the lone pairs of oxygen atoms enhances the tetrahedral network of the hydrogen bonds. As TIP5P is generally thought of as too structured, the SWM4-NDP model result is an improvement with respect to that of TIP5P.

The correlation functions of the hydrogen bonds formed in water or between carbonate and water show some obvious similarities. First of all, there exist several superimposed time scales. The first time scale is extremely fast: already at 0.1 ps the normalized correlation functions are around 0.8–0.9. This means that a significant part of the hydrogen bonds have an extremely short lifetime. This is the well-known libration motion
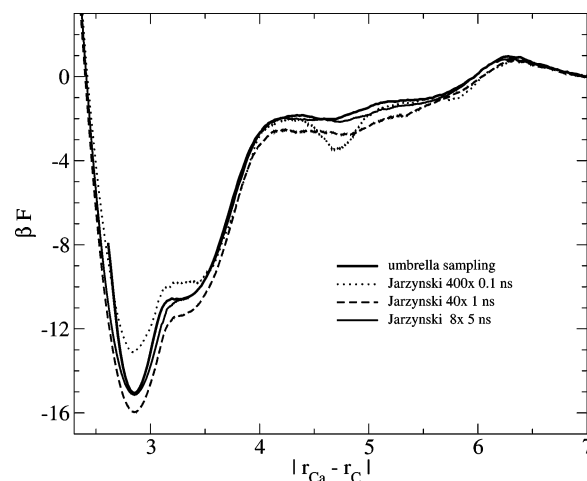
of water molecules.[37] Then, both types of hydrogen bonds exhibit rather slow decay that cannot be fitted by single-exponential functions. The characteristic time of the hydrogen bonds formed with carbonate is 36 ± 6 ps at 300 K and 14 ± 1 ps at 365 K. The uncertainty is due to the difficulty of gathering statistics for a single solvated ion. Because of the strong Coulomb attraction between the O_c atom and the H of water, the correlation time of the carbonate–water hydrogen bonds is much longer than that of the hydrogen bonds in water.

The long-lived hydrogen bonds formed between the carbonate and the solvent reduce the self-diffusion of the ion in water. The diffusion coefficient is evaluated from a 12 ns simulation as being $0.60 10^{-5} cm^2 \cdot s^{-1}$ at 300 K and $1.74 10^{-5} cm^2 \cdot s^{-1}$ at 365 K.

In general, we have shown that the building blocks of $CaCO_3$ form stronger bonds to the solvent than the standard H-bonds in water. The high stability of the solvation shells of both the ions limits their diffusivity, especially at low temperatures. This reduced diffusivity may play a critical role in the process of aggregation and precipitation.

IV. Solvated Heteroion Pair

Performing standard MD simulations of a single unit of $CaCO_3$ in water, we observe that the cation–anion pair tends to bind and never dissociates within the typical simulation time of a few nanoseconds, even at the higher temperature considered in this study (365 K). On the contrary, for ion pairs with weaker charges, such as NaCl, the dissociated situation is more favorable.[39] In the present section, we investigate the binding of hydrated calcium carbonate, which can give a first hint toward explaining the very low solubility of $CaCO_3$.

We compute the free energy with umbrella sampling as a function of the distance between the carbon of a carbonate and the calcium $|r_C - r_{Ca}|$ solvated in a box of 100, 262, or 520 water molecules. The latter corresponds to a concentration as low as 0.1 M. The constant for the harmonic bias potential is set to the rather large value of 2.0 eV/Å^2, since the free energy profile shows steep sections, and we put a window every 0.25 Å. We equilibrate every window for 50 ps and compute the distribution over the 500 ps. The free energy profile is obtained using the weighted histogram analysis method (WHAM) as implemented in ref 40 and is plotted with a thick line in Figure 7.

Solvation of Calcium Carbonate in Water

J. Phys. Chem. B, Vol. 111, No. 42, 2007 **12225**

Since for all the concentrations, the free energy plots are consistent within 0.5 kcal/mol, we show only the one obtained for the most concentrated system.

We also evaluate the same free energy profile exploiting the Jarzynski equality[41] and computing the exponential average of the work performed in nonequilibrium simulations to dissociate the pair:

$$\exp(-\beta F(s)) = \langle \exp(-\beta W(s)) \rangle \qquad (3)$$

where $\beta = 1/kT$, and $W(s)$ is the work needed to bring the system to position s. We therefore perform several runs, steering the ions from dissociated to associated by continuously moving the center s_0 of the bias potential U_{bias} to 2 Å. The total simulated dynamics is 40 ns, using either 400 runs of 0.1 ns (dotted line in Figure 7), 40 runs of 1 ns (dashed line), or 8 runs of 5 ns (thin line). The overall agreement between umbrella sampling and the Jarzynski approach is good; it becomes ever better as the adiabatic limit of the infinitely slowly moving bias potential is approached. These findings appear to be quite general.[42] When reaching the thermodynamic integration limit, the main advantage of the Jarzynski method (i.e., the possibility to run several independent calculations) is completely lost. In the present case, umbrella sampling should be preferred: it provides the converged result faster and allows parallelization over the umbrellas.

The free energy profile of Figure 7 clearly demonstrates that the associated configuration is preferred over the dissociated one. The association process does not experience any significant barrier. One may argue that the distance between the ions may not be a good collective variable, but this possibility can be safely ruled out, since the association of CaCO₃ is easily observed in unbiased MD simulations. This means that there is no free-energy barrier to prevent the fast binding. The correspondence between the results obtained by umbrella sampling and those obtained by nonequilibrium steered dynamics validates the free energy profile represented in Figure 7. A free energy difference of 15 kT between associated and dissociated at 300 K shows that the occurrence of dissociate calcium and carbonate ions would be very low, even at low concentrations. For instance, in a crude model where the free-energy profile is modeled by a square well of depth 15 kT between 2.6 and 3.6 Å, infinity below 2.6 Å, and 0 beyond 3.6 Å, the associated proportion is 99.9% for a concentration of ions of 10^{-3} M. This confirms our primary findings that once Ca^{2+} and CO_3^{2-} have formed a bound pair, it is impossible to observe the subsequent dissociation on the time scale of MD simulations.

Our MD simulations predict a strong binding between solvated calcium and carbonate, which is in agreement with the very low solubility observed experimentally. To further assess the validity of this qualitative result, it is valuable to inquire what an analogous force field would predict for a heteroion pair formed by CO_3^{2-} and a monovalent cation. This test is motivated by a recent MD study that stated that Cs^+ and CO_3^{2-} do bind in aqueous solution at higher concentration (1.5 M).[5] Therefore, we consider a potassium ion K^+, which has about the same atomic weight as calcium, and we investigate the binding of K^+ and CO_3^{2-}. Experimentally, K_2CO_3 is known to be soluble in water. The short-range interaction between K^+ and H_2O is modeled via a Lennard–Jones potential with the parameters taken from ref 20. In contrast with ref 20, we do not introduce a shell on K^+, since the polarizability of potassium is low. The interaction between K^+ and CO_3^{2-} is the same as that for Ca^{2+} and CO_3^{2-}, except that the charge of K^+ is fixed to one. This parametrization gives the correct binding energy and equilibrium
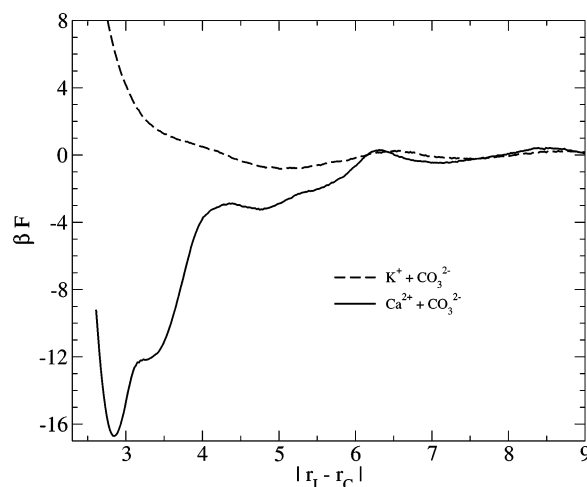

Figure 8. Free energy profile in units of kT as a function of the distance between K^+ or Ca^{2+} and C, calculated for a cation–anion pair with 262 water molecules at 300 K. The solid line corresponds to calcium, and the dashed one corresponds to potassium.

distance of the KCO₃ and KH₂O pairs in the gas phase, as shown in Table 2. The agreement is of the same quality as that for calcium carbonate.

Using this force field, umbrella sampling is performed with the same parameters used for the Ca^{2+} CO_3^{2-} ion pair in order to evaluate the free energy as a function of the distance between K^+ and CO_3^{2-}, represented in Figure 8. As opposed to calcium carbonate, the potassium carbonate does not present any bound state in the 2.8 Å distance area, which is the equilibrium distance in the gas phase. Instead, the free energy profile is completely flat between 3 and 9 Å, with only structures on the order of kT. In conclusion, the type of force field in use is able to discriminate between the species that experience heteroion pairing and the ones that do not. The strength of the Coulomb interaction between the two ions is crucial to explain the difference when Ca^{2+} is substituted by K^+. Only for Ca^{2+} (and divalent cations in general) is the ion–ion attraction large enough to compensate the fewer hydrogen bonds formed with the solvent. In addition to the electrostatic term, the binding is favored by the entropy gained by releasing water in the solvation shells of both Ca^{2+} and CO_3^{2-}. This finding is supported by a recent study of the binding of Ca^{2+} to carboxylate groups of polyacrylate,[43] as opposed to the non-binding behavior of Na^+.

Given the high probability of the occurrence of CaCO₃ pairs in water, it is important to study their solvation shell. The hydration shell of CaCO₃ is represented in Figure 9. The data presented here are extracted from a 10 ns simulation at 300 K. The hydration shell is extremely structured. Around the calcium ion, five preferred sites can be distinguished in panel a. In panel b, one can observe that, around the carbonate ion, the water molecules are localized in four sites linked to the O_c opposite to Ca^{2+} and in two sites related to the two O_c atoms connected to Ca^{2+}. Furthermore, some of the sites that were found to be populated in the single carbonate ion case are no longer visited by water in the case of the bound pair. Instead, the location of the water molecules in aqueous solution is strikingly similar to their position in the hexahydrated mineral (ikaite). In panel e of Figure 9, we have reported the probability isosurfaces of O_w for an MD run for ikaite at low temperature (10 K). The overall structure of the H₂O molecules greatly resembles the liquid case, even though the CaCO₃ units are stacked in a packed way in the crystal and though the water molecules are shared between different CaCO₃ units. The O_c opposite to Ca^{2+} is involved in the formation of four hydrogen bonds, whereas the other two
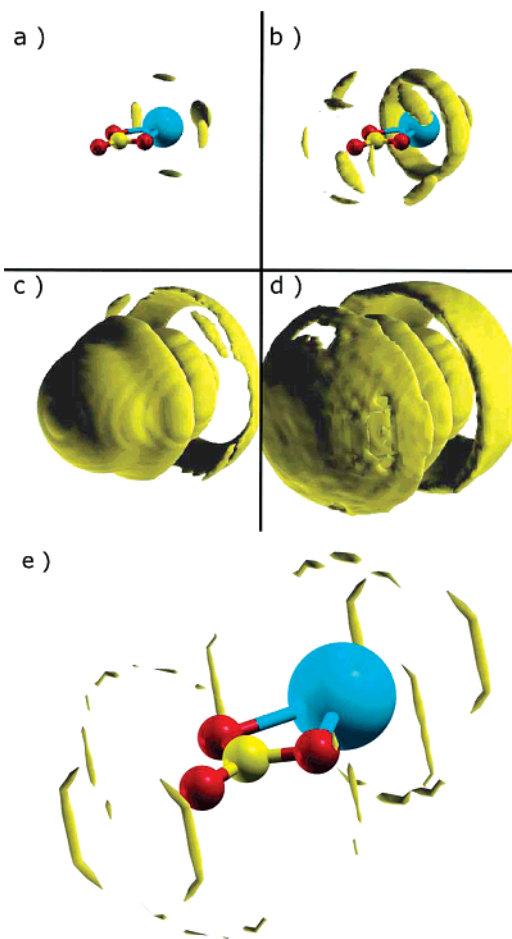
Figure 9. Isoprobability surfaces for the localization of O_w in the frame of the $CaCO_3$ unit. Panels a−d correspond to decreasing values for the isosurface in the solvated case. Panel e corresponds to an isosurface in the hydrated mineral, ikaite.

O_c atoms participate in two hydrogen bonds. Panels c and d of Figure 9 describe the second solvation shell. This shell is extremely structured in the region where Ca^{2+} and CO_3^{2-} are bound: there is a large portion of space, in the region perpendicular to the Ca−CO bond, where the water molecules are literally excluded.

Since the bound pair is much more probable than the separated ions, even at low concentration, the diffusion of this building block may be one of the limiting steps of the kinetics of nucleation. We then evaluate the diffusion coefficient of a bound unit of $CaCO_3$ out of a 12 ns run: $0.46 10^{-5} cm^2 \cdot s^{-1}$ at 300 K and $1.57 10^{-5} cm^2 \cdot s^{-1}$ at 365 K. The diffusivity of the pair is of the same order of magnitude as the single ions alone (Ca^{2+} and CO_3^{2-}), even though the $CaCO_3$ unit is heavier. It appears that the environment surrounding the calcium carbonate pair is more flexible and does not limit the diffusion as much as it does for the charged species.

V. Conclusion

The classical force field we have presented here allows for an accurate description of calcium and carbonate in different environments, clusters, minerals, and ions in water. We have employed it to elucidate the properties of the solvated ions Ca^{2+}, CO_3^{2-}, and the solvated $CaCO_3$ unit. While the study of calcium confirmed the quality of our force field, the study of carbonate gives important information in the little-explored topic of the solvation properties of complex anions. From our classical MD, we conclude that, on average, the water solvent forms about

12 hydrogen bonds with the carbonate solute, with a long relaxation time of 36 ps at room temperature. The solvation shell of carbonate is very structured: not only is the first shell not isotropic, but the second shell also shows sharp three-dimensional structures. In particular, an interesting exclusion area, located on top of the carbon atom of carbonate, can be observed. This hydrophobic point may play a crucial role in the nucleation of calcium carbonate, as the CO_3^{2-} will tend to minimize the contact between water and its hydrophobic region. Interestingly, two of the three $CaCO_3$ minerals commonly found in nature (aragonite and vaterite) show the same common feature of having the carbonate units piled on top of one another, and thereby reducing the exposure of their hydrophobic area to water. Our study of the $CaCO_3$ unit demonstrates the strong binding between the calcium and the carbonate ($\sim$8 kcal/mol) in water and the fact that the pair itself is not soluble in water. This is consistent with the very low solubility of calcium carbonate.

The present paper opens the way to the understanding of the microscopic mechanisms involved in the nucleation of calcium carbonate in solution. Because of the large binding between the calcium and carbonate, we expect that the precipitation of calcium carbonate is only kinetically limited by the low diffusivity of its building blocks. These two combined features make the formation of ordered minerals a very slow process that evolves through several intermediates.

References and Notes

(1) Addadi, L.; Raz, S.; Weiner, S. *Adv. Mater.* **2003**, *15*, 959.
(2) Schlomach, J.; Quarch, K.; Kind, M. *Chem. Eng. Technol.* **2006**, *29*, 215.
(3) Wang, X.-B.; Yang, X.; Nicholas, J. B.; Wang, L.-S. *Science* **2001**, *294*, 1322.
(4) Vchirawongkwin, V.; Rode, B. M.; Persson, I. *J. Phys. Chem. B* **2007**, *111*, 4150.
(5) Mason, P. E.; Neilson, G. W.; Dempsey, C. E.; Brady, J. W. *J. Am. Chem. Soc.* **2006**, *128*, 15136.
(6) Schwenk, C. F.; Loeffler, H. H.; Rode, B. M. *J. Chem. Phys.* **2001**, *115*, 10808.
(7) Bakó, I.; Hutter, J.; Pálinkás, G. *J. Chem. Phys.* **2002**, *117*, 9838.
(8) Naor, M. M.; van Nostrand, K.; Dellago, C. *Chem. Phys. Lett.* **2003**, *369*, 159.
(9) Lightstone, F. C.; Schwegler, E.; Allesch, M.; Gygi, F.; Galli, G. *Chem. Phys. Chem.* **2005**, *6*, 1745.
(10) Megyes, T.; Bakó, I.; Bálint, S.; Grósz, T.; Radnai, T. *J. Mol. Liq.* **2006**, *129*, 63.
(11) Hewish, N. A.; Neilson, G. W.; Enderby, J. E. *Nature* **1982**, *297*, 138.
(12) Fulton, J. L.; Heald, S. M.; Badyal, Y. S.; Simonson, J. M. *J. Phys. Chem. A* **2003**, *107*, 4688.
(13) de Leeuw, N. H.; Parker, S. C. *Phys. Rev. B* **1998**, *58*, 13901.
(14) de Leeuw, N. H.; Parker, S. C. *Phys. Chem. Chem. Phys.* **2001**, *3*, 3217.
(15) Soper, A. K. *Chem. Phys.* **2000**, *258*, 121.
(16) Pavese, A.; Catti, M.; Price, G. D.; Jackson, R. A. *Phys. Chem. Miner.* **1992**, *19*, 80.
(17) Archer, T. D.; Birse, S. E. A.; Doye, M. T.; Redfern, S. A. T.; Gale, J. D.; Cygan, R. T. *Phys. Chem. Miner.* **2003**, *30*, 416.
(18) Frisch, M. J.; Trucks, G. W.; Schlegel, H. B.; Scuseria, G. E.; Robb, M. A.; Cheeseman, J. R.; Montgomery, J. A., Jr.; Vreven, T.; Kudin, K. N.; Burant, J. C.; Millam, J. M.; Iyengar, S. S.; Tomasi, J.; Barone, V.; Mennucci, B.; Cossi, M.; Scalmani, G.; Rega, N.; Petersson, G. A.; Nakatsuji, H.; Hada, M.; Ehara, M.; Toyota, K.; Fukuda, R.; Hasegawa, J.; Ishida, M.; Nakajima, T.; Honda, Y.; Kitao, O.; Nakai, H.; Klene, M.; Li, X.; Knox, J. E.; Hratchian, H. P.; Cross, J. B.; Bakken, V.; Adamo, C.; Jaramillo, J.; Gomperts, R.; Stratmann, R. E.; Yazyev, O.; Austin, A. J.; Cammi, R.; Pomelli, C.; Ochterski, J. W.; Ayala, P. Y.; Morokuma, K.; Voth, G. A.; Salvador, P.; Dannenberg, J. J.; Zakrzewski, V. G.; Dapprich,

Solvation of Calcium Carbonate in Water

J. Phys. Chem. B, Vol. 111, No. 42, 2007 **12227**

S.; Daniels, A. D.; Strain, M. C.; Farkas, O.; Malick, D. K.; Rabuck, A. D.; Raghavachari, K.; Foresman, J. B.; Ortiz, J. V.; Cui, Q.; Baboul, A. G.; Clifford, S.; Cioslowski, J.; Stefanov, B. B.; Liu, G.; Liashenko, A.; Piskorz, P.; Komaromi, I.; Martin, R. L.; Fox, D. J.; Keith, T.; Al-Laham, M. A.; Peng, C. Y.; Nanayakkara, A.; Challacombe, M.; Gill, P. M. W.; Johnson, B.; Chen, W.; Wong, M. W.; Gonzalez, C.; Pople, J. A. *Gaussian 03*, Gaussian, Inc.: Wallingford, CT, 2004.

(19) Stefanovich, E. V.; Boldyrev, A. I.; Truong, T. N.; Simons, J. *J. Phys. Chem. B* **1998**, *102*, 4205.

(20) Lamoureux, G.; Harder, E.; Vorobyov, I. V.; Roux, B.; MacKerell, A. D., Jr. *Chem. Phys. Lett.* **2006**, *418*, 245.

(21) Jorgensen, W. L.; Chandrasekhar, J.; Madura, J. F.; Impey, R. W.; Klein, M. L. *J. Chem. Phys.* **1983**, *79*, 926.

(22) Lamoureux, G.; Roux, B. *J. Phys. Chem. B* **2006**, *110*, 3308.

(23) Pilati, T.; Demartin, F.; Grammaccioli, C. M. *Acta Crystallogr. B* **1998**, *54*, 515.

(24) Effenberger, H. *Monatsh. Chem.* **1981**, *112*, 899.

(25) Hesse, K. F.; Suess, E. *Z. Kristallogr.* **1983**, *163*, 227.

(26) de Leeuw, N. H.; Parker, S. C. *J. Chem. Soc., Faraday Trans.* **1997**, *93*, 467.

(27) Smith, W.; Leslie, M.; Forester, T. R. *DL_POLY*, version 2.16; Daresbury Laboratoy: Daresbury, England.

(28) Smith, W.; Forester, T. *J. Mol. Graphics* **1996**, *14*, 136.

(29) Bussi, G.; Donadio, D.; Parrinello, M. *J. Chem. Phys.* **2007**, *126*, 014101.

(30) Car, R.; Parrinello, M. *Phys. Rev. Lett.* **1985**, *55*, 2471.

(31) Mitchell, P. J.; Fincham, D. *J. Phys.: Condens. Matter* **1993**, *5*, 1031.

(32) Kofala, J. *J. Chem. Phys.* **2005**, *122*, 164105.

(33) Salmon, P. S.; Howells, W. S.; Mills, R. *J. Phys. C: Solid State Phys.* **1987**, *20*, 5727.

(34) Koneshan, S.; Rasaiah, J. C.; Lynden-Bell, R. M.; Lee, S. H. *J. Phys. Chem. B* **1998**, *102*, 4193.

(35) Kusalik, P. G.; Svishchev, I. M. *Science* **1994**, *265*, 1219.

(36) Starr, F. W.; Nielsen, J. K.; Stanley, H. E. *Phys. Rev. E* **2000**, *62*, 579.

(37) Luzar, A.; Chandler, D. *Nature* **1996**, *379*, 55.

(38) Raiteri, P.; Laio, A.; Parrinello, M. *Phys. Rev. Lett.* **2004**, *93*, 087801.

(39) Geissler, P. L.; Dellago, C.; Chandler, D. *J. Phys. Chem. B* **1999**, *103*, 3706.

(40) Chodera, J. D.; Swope, W. C.; Pitera, J. W.; Seok, C.; Dill, K. A. *J. Chem. Theor. Comput.* **2007**, *3*, 26.

(41) Jarzynski, C. *Phys. Rev. Lett.* **1997**, *78*, 2690.

(42) Oberhofer, H.; Dellago, C.; Geissler, P. L. *J. Phys. Chem. B* **2005**, *109*, 6902.

(43) Bulo, R. E.; Donadio, D.; Laio, A.; Molnar, F.; Rieger, J.; Parrinello, M. *Macromolecules* **2007**, *40*, 3437.